TELKOMNIKA Telecommunication, Computing, Electronics and Control
Vol. 19, No. 3, June 2021, pp. 983~990
ISSN: 1693-6930, accredited First Grade by Kemenristekdikti, Decree No: 21/E/KPT/2018
DOI: 10.12928/TELKOMNIKA.v19i3.18794

High-resolution rotor-position detection for green vehicle drives at halt condition with statistical view

Mazen M. A. Al Ibraheemi[1], Fatih J. Anayi[2], Zainb Hassan Radhy[3], Hayder Al Ibraheemi[4]
[1]Department of Electronics and Communications Engineering, Faculty of Engineering, University of Al-Qadisiyah, Iraq
[2]Wolfson Centre for Magnetics, Cardiff University, United Kingdom
[3]College of computer science and information technology, University of Al-Qadisiyah, Iraq
[4]Faculty of Technical Engineering, Islamic University, Iraq

Article Info

Article history:

Received Sep 2, 2020
Revised Nov 14, 2020
Accepted Nov 25, 2020

Keywords:

Halt position
Interior permanent magnet synchronous machine
Memory and address lines
Pulse injection
Rotor position detection

ABSTRACT

Considerations around environmental pollution and green energy usage have led to environmentally-friendly machines being used in many industrial applications. Permanent magnet (PM) machines are the best solution to substitute the pollutant diesel-powered machines. In such machines, rotor position detection is crucial for safe startup operating. Meanwhile, encoderless controllers have become more reliable, over the years, in supporting the operation of PM machines. The key point, presented by this paper, is to introduce an improved positioning model to detect the rotor-position of interior permanent magnet synchronous machine at halt condition. To verify this objective, only two short duration pulses were injected into the stator windings. Then, the corresponding terminal voltage and current responses were measured and employed to create two memory address lines. Thereby, the memory cells, which contain the rotor position information, could be accessed. This detection model makes a significant improvement in rotor positioning detection of high resolution (1 degree) which represents lower value than most verified results in literature. The model was simulated and tested in a MATLAB/Simulink environment and shows an approximate accuracy 95%. Additionally, the statistical analysis was also employed to support the work outcomes.

Corresponding Author:

Mazen M. A. Al Ibraheemi
Department of Electronics and Communications Engineering,
Faculty of Engineering
University of Al-Qadisiyah
Iraq
Email: mazen.ali@qu.edu.iq

1. INTRODUCTION

Environmental pollution represents a massive task in modern life. Power engines of diesel cars play an important role in negative contributing to air pollution. Gradually, environmentally-friendly electric cars, based on permanent magnet synchronous machines (PMSM), have proceeded to substitute vehicle engines which considered as a source of such pollution [1-3]. PMSMs have an essential role in the wide range of green industrial applications, due to their promising features such as low consumption of fuel, significant reduction in carbon dioxide (CO_2) emissions, more reliable, better power-to-size ratio and more rapid speed reaction [4-9]. However, some drawbacks are also companying the use of PMSM such as it cannot be directly derived from the alternating voltage source. It needs a complicated control system to do so, which makes it an expansive

technology. Anyhow, the permanent magnet motors are preferable in many industrial fields, from home appliances to complicated industrial processes. So, the electrical vehicles (Evs) employ permanent magnet (PM) motors as an efficient prime drive to generate the required high torque and speed [10-12]. Figure 1 highlights the leading position of PM motors as a prime, or steering, drives in electrical vehicles (EVs) [10].

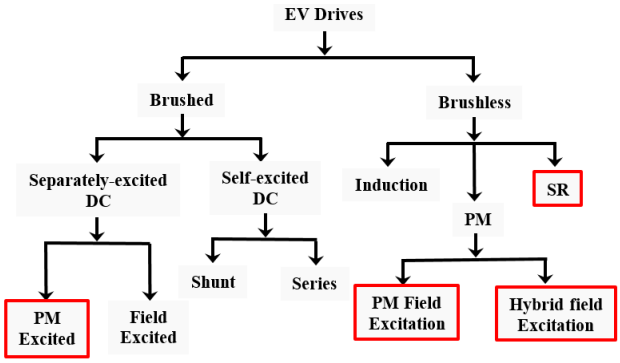

Figure 1. Various types of the EV drives

The key point to the optimal operation of the PM motors is the precise commutation process. This process is highly dependent on the accuracy of the motor rotor position detection (RPD). Consequently, the accurate RPD is considered as a crucial impact in maintaining optimum running of PM motors [13]. Particularly, at halt condition, the successful RPD preserves a reasonable primary operation and avoids reverse running or stall of rotor, while it ensures soft running with minimum torque ripple at low and high motor speeds. Therefore, various researching efforts have been achieved to preform the RPD over a wide speed range of motor running, from halt to high speed [11, 14].

A wide field of those researching efforts has concerned the permanent magnet synchronous motors PMSM, by its twofold, the interior permanent magnet synchronous machine (IPMSM) and surface mounted permanent magnet synchronous machine (SMPMSM). K. Ravikumar Setty *et al.* [15] presented a classification to the methods of RPD, which still adopted up to date. Although the majority of RPD methods, or studying the PMSM features, have a common point that they based on tracking the rotor magnetic saliency, such as in [16, 17], they differ in field of application. This application field is related to speed of motor; standstill (halt), low or medium/high speed. Whereas, the minority of RPD methods have different points of view for achieving the task [18-20]. Gradually, the RPD becomes so important to PMSM such that one of the control schemes of PMSM controls, called "vector control", is based on it. Away from RPD, another control scheme, called "Scaler Control" scheme, depends on the magnitude and frequency of stator applied voltages [21].

The pulse injection method, which is employed in this work, stands within the category of RPD methods, given by [15], as the most suitable to be used in vector control of brushless dc motors, BLDCs. By this method, the yielded impulse responses are compared to each other to generate a sectoral division to the whole spatial positions of permanent magnet rotor [22]. Although a low resolution RPD always incomes by this method, almost 30-degree resolution [23], it is sufficient to run the BLDC. In contrast, for PMSM applications, the low resolution RPD represents an essential drawback as it may lead to deteriorate the performance of motor drive system [24]. In literature, some researchers tried to address this drawback. For example, Q. Ni *et al.* [24] proposed a solution based on merging the statistical approach least squares method (LSM), with a proper positioning and speed estimator. However, those researching efforts may suffered from complexity and relatively high cost. Nevertheless, the pulse injection method was efficiently used by [25] to detect the rotor position of SMPMSM through injection of three pulses into the motor stator windings and testing the terminal voltage responses. This reference also presented a comparative scheduling for the results obtained by other relevant works. It may be worth to mention that the technique of pulse injections has been also used in driving systems of other motors rather than PMSM. For instance, X. Zhou *et al.* [16] applied this technique on electromagnetic machine of doubly salient to predicate the rotor position through influencing the relation between the rotor sector and the minimum value of self-inductance.

This paper introduces an approach for interior permanent magnet synchronous machine (IPMSM) rotor position detection, RPD. The work specifically deals with the motor in halt condition without any form of positioning sensor. It bases on influencing the inductance variations in the stator windings of IPMSM when they excited by applying two cascaded short pulses and employing the effect of rotor high saliency. Although,

the presented model has suffered from voltage uncertainty, it has been a good attempt to solve the obstacle of cost and complexity. Comparing with previous works, the main contributions, made by this work, is to implement a RPD of high resolution at 1 degree. Remaining of this paper is organized as following: section two highlights the paper research methodology. It includes two subsections which details the work in this paper. The results and their discussion are explored in section three. Finally, section four summarises the conclusions.

2. RESEARCH METHOD

The proposed scheme in this paper is based on creating a memory structure whose cells are previously loaded with the 360 rotor positions, RPs. Then, measurements of the motor terminal voltages and currents, at each RP, should provide two numbers. The numbers are utilized as address lines, x and y, to access the memory cells. Thereby, the RP can be detected through its corresponding effect on motor terminal output voltages. Figure 2 highlights this topic. More details about the methodologies of measuring terminal voltages and coil currents are outlined in the next two sub-sections.

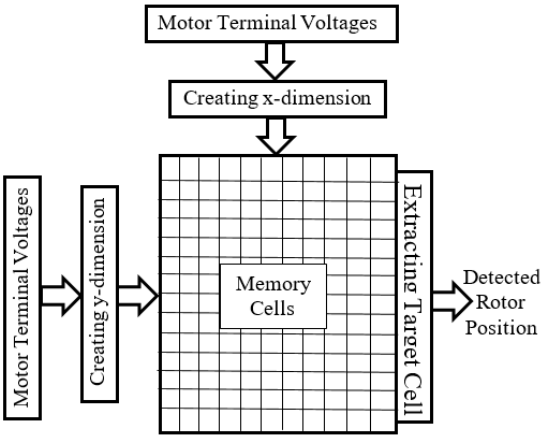

Figure 2. Basic concept of RPD

2.1. Voltage measurements and formatting the x-address line

The voltage measurements are employed to format the memory x-address. At halt condition and for test purposes, the three stator coils (A, B and C) of a PM motor can be combined to form a series loop of two coils, whilst the third is left an open circuit, oc, of a free terminal. Accordingly, Figure 3 shows all possible series loops. The series-coils can be excited by a testing pulse of a short duration and the corresponding impulse responses on the both excited coils can be monitored by the free terminal of the third non-excited coil. For instant, Figure 4 shows exciting the series-coils A-C by the first testing pulse and the corresponding voltage drops during the forward and flyback periods, $(V_{C1})_{FW}$ and $(V_{A1})_{FBK}$ respectively. The currents of those periods, I_{FW} and I_{FBK}, are also shown. The Figure 4 action is repeated by applying the second testing pulse on the series coils A-B. Consequently, two additional voltage drops are measured $(V_{B2})_{FW}$ and$(V_{A2})_{FBK}$. Thereby, the voltages at the motor terminals B and C are measured, compared, decoded to eventually format the x-address line. Figure 5 illustrates the basic steps of achieving this part.

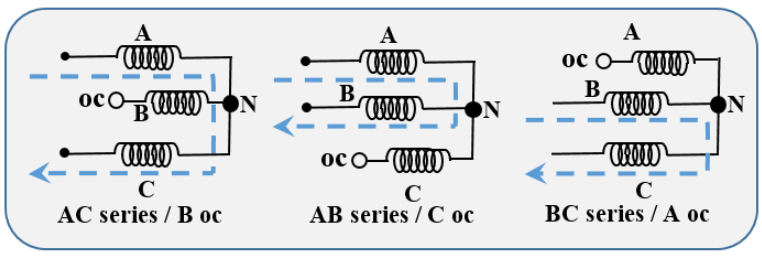

Figure 3. The three configurations of stator coils series loops

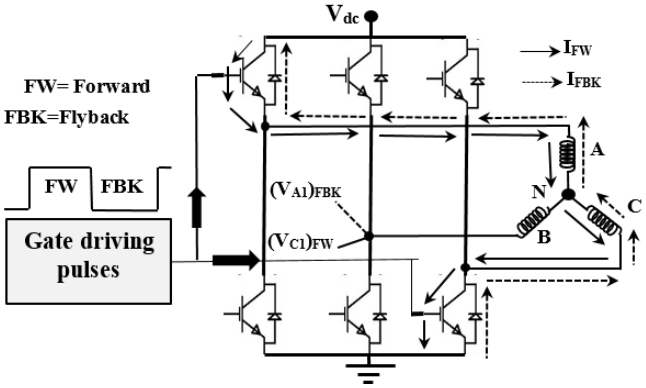

Figure 4. Exciting of coils A and C by the first testing pulse and the flyback reaction

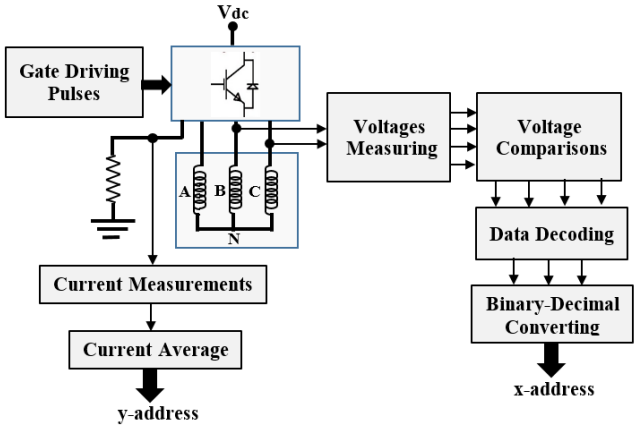

Figure 5. Process of formatting the memory address lines

2.2. Current measurements and formatting the y-address line

The current measurements are designated to format the y-address of the memory given by Figure 2. Each testing pulse produces a short duration current response in forward direction which is symbolled in Figure 4 by solid arrows. When the active duration of this pulse elapses, a flyback current flowing in reverse direction, through the IGBT flyback diodes. This current is symbolled in Figure 4 by dashed arrows. Regarding Figure 4 as a case study, the currents follows the (1) and (2) respectively.

$$I_{FW} = \frac{V_{dc}}{R}\left(1 - e^{-\frac{R}{L}t}\right) \quad (1)$$

$$I_{FBK} = \frac{V_{dc}}{R} e^{-\frac{R}{L}t} \quad (2)$$

Where V_{dc} is the dc bus voltage, R is the total resistance of the series-coils A-C, $R_A + R_c$ and L is the equivalent self-inductance $L_A + L_C$. Figure 6 shows the two testing pulses and the corresponding two current responses. Then by Figure 5, the first pulse causes the voltage drop $(V_{C1})_{FW}$ which can be expressed as (3).

$$(V_{C1})_{FW} = I_{FW} R_C + L_C \frac{dI_{FW}}{dt} \quad (3)$$

As the range of time variant is within the pulse width, which is too short to display the full range of current growth of (1), only the linear part of this equation will be visible as it is highlighted in Figure 6. The linear part can be expressed by the equation y=mx+c, where m and c represent the equation slope and constant respectively. Therefore, the slope m equals the current variation $\frac{dI_{FW}}{dt}$ which permits to write a formula for current, according to (3), as:

$$I_{FW_1} = \frac{(V_{C1})_{FW} - mL_C}{R_C} \quad (4)$$

In (4), only the voltage $(V_{C1})_{FW}$ has a relation with the angle of rotor position. Therefore, the value of current average, I_{av}, will be a function to the angle position of rotor. A narrow testing pulse of very small fraction of the motor time constant (L/R) allows to run the proposed model over a wide range of motor rating currents.

Figure 6 illustrates the first and second applied testing pulses. The total period is 300μsec and the active high duration is 150 μsec. The pulses are applied on the series-coils A-C and A-B respectively. The figure also shows the corresponding shapes of current responses, the forward (FW) and flyback (FBK) currents. The average of $(I_{AC})_{FW}$, highlighted by the shaded area, was chosen in this work to format the y-address. The procedure of formatting the y-address is briefly mentioned in Figure 5. To calculate the average current value, the proposed model, firstly, defines the current period through which the average to be found. Secondly, it applies the following equation to complete the task.

$$I_{av} = \frac{1}{T_{period}} \int I_{FW1} dt \quad (5)$$

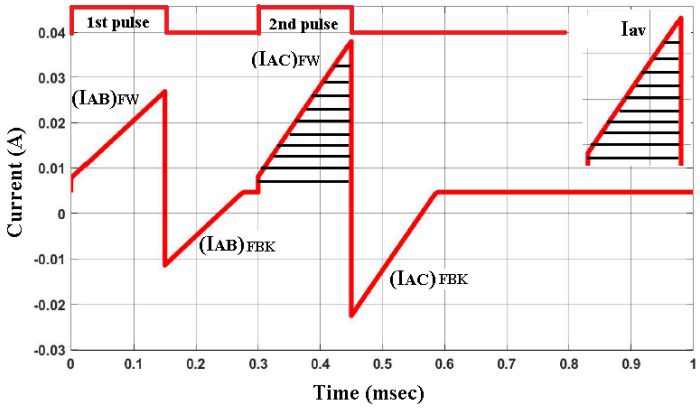

Figure 6. The applied testing pulses and the corresponding current responses

3. RESULTS AND ANALYSIS

Concept of the paper was implemented via a MATLAB model approach. Figure 7 shows the MATLAB/Simulink approach to simulate and run the proposed view of this work. To meet the work objectives, the exact angular positions of the target permanent magnet rotor were stored in the cells of the memory block as shown in Figure 2. The memory was simulated be a 2-D lookup table from the Simulink library. Each cell in the memory is referred to its location via two address buses. First is the x-address line which can be obtained from the terminal voltage measurements and the corresponding six sectors of rotor spatial. This address line divides the memory into six portions, each of which determines the proper position of rotor within the specified sector. Second is the y-address line whose value is determined by the current average as it is explained in section 2.2. Thereby, the target memory cell is activated by intersection of the two address lines, sectors and current average lines (x and y address lines).

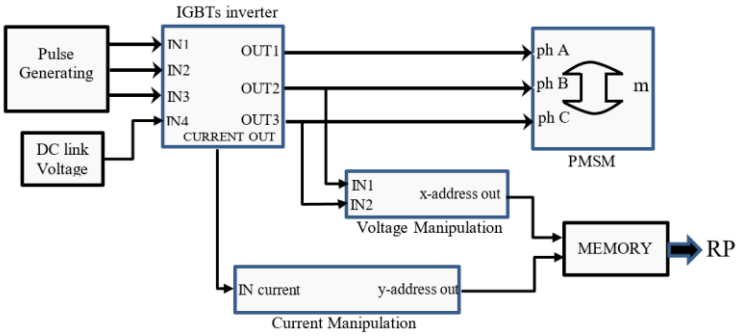

Figure 7. The MATLAB/Simulink approach

Figure 8 shows the results of voltage measurements by the MATLAB Simulink modelling shown in the previous figures. The four voltages $(V_{C1})_{FW}$, $(V_{A1})_{FBK}$, $(V_{B2})_{FW}$ and $(V_{A2})_{FBK}$ were obtained when the rotor was setting at position 45^0. Measuring of those four voltages was performed for RPs varying from 0^0 to 360^0. The corresponding resultant voltage values are shaped as presented in Figure 9. The figure also shows the rotor spatial divisions into sectors with respect to the comparative values of the measured voltages.

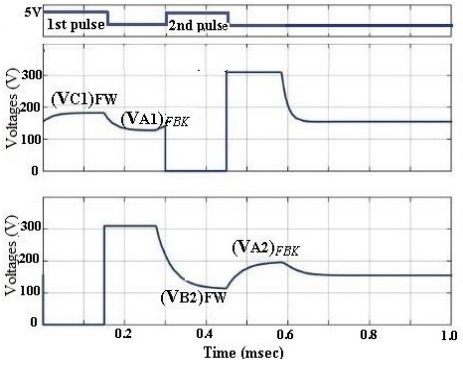

Figure 8. The measured voltages at RP of 45°

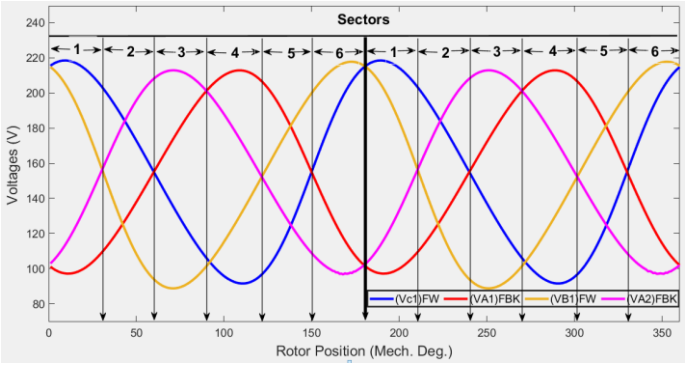

Figure 9. The measured voltages and sector regions over the whole range of rotor spatial

Accordingly, three considerable comparisons can be achieved between each two of the measured voltages, $(V_{C1})_{FW}$, $(V_{A1})_{FBK}$, $(V_{B2})_{FW}$ and $(V_{A2})_{FBK}$. These comparisons create predictable divisions to the rotor electrical angular position into six sectors, each of 30^0 angular width, as shown in Table 1. The sectors numbering are exploited to decode the x-address of the memory given by Figure 2.

Table 1. Coding of voltage comparisons into x- address line

Voltage's comparisons	Logic states of sectors:					
	1	2	3	4	5	6
$(V_{C1})_{FW} \geq (V_{A1})_{FBK}$	1	1	0	0	0	1
$(V_{B2})_{FW} \geq (V_{A2})_{FBK}$	1	0	0	0	1	1
$(V_{C1})_{FW} \geq (V_{B1})_{FW}$	1	1	1	0	0	0
$(\text{x-address})_2$	111	101	001	000	010	110
$(\text{x-address})_{10}$	7	5	1	0	2	6

As the x and y addresses become available from the voltage and current measurements respectively, the memory, given by Figure 2, is accessible to extract the different RPs. The straight line in Figure 10 represents the detection results of RP. It is obviously clear that the proposed approach failed in detection of the correct position at some rotor angles. The points of highest errors, 1 through 4, are indicated on this figure. The rate of error at each of these points is individually evaluated by the relation:

$$Rate\ of\ error\ at\ each\ point\ = \frac{Detected\ position - Actual\ position}{Actual\ position} \times 100\% \quad (6)$$

Consequently, the rate of error, at the error points 1 through 4, are found to be 1.44%, 1.89%, 4.1% and 12.51% respectively. The resultant error is interpreted by a deviation in estimating the correct sector number at which the RP locates. These deviations especially take place at the boundaries among the sectors where the measured voltage values become too close to be distinguished by the voltages comparing block shown in Figure 5. Therefore, an error in x-addressing occurs which causes to shift the detection process to the neighbour memory cells.

Figure 11 graphically explores all the errors in detecting the RP over the whole 360^o rotor space. Some of errors are too low to be noticeable on the figure. Anyhow, the model indicated 17 overall errors, out of 360 in detecting the exact angle position of the rotor. This number of errors makes the total error rate of the proposed model equals to 4.7%.

Figure 12 shows a statistical analysis for the values of x and y addresses. The valuable statistic in this figure is the standard deviation (std) where its value gives the model ability to distinguish between the sectors numbering values and the average current values. Table 2 illustrates the various parameters of the motor

under simulation, where the default values of the motor specifications, given by the MATLAB, were used in the module tests.

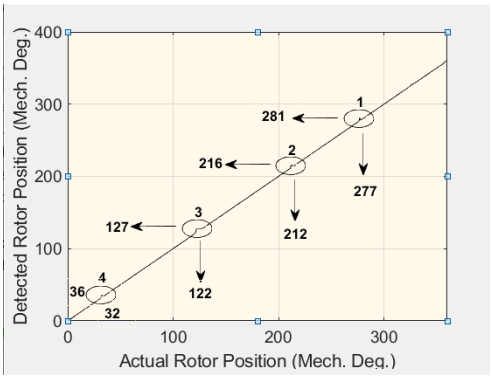

Figure 10. The detected RPs versus the actuals

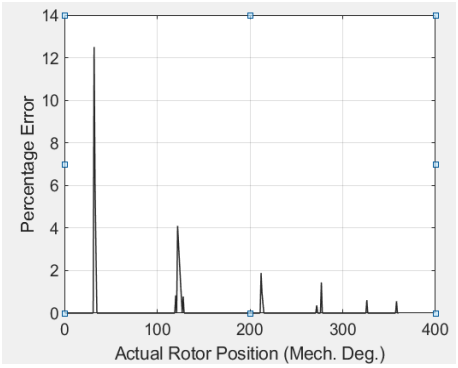

Figure 11. Rate of errors over the whole RP space

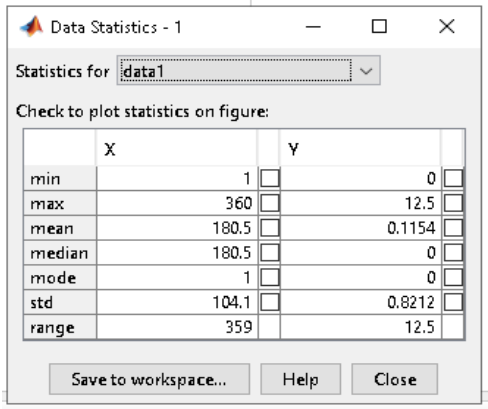

Figure 12. Statistics analysis of x and y addresses

Table 2. Properties of motor under test

Parameter	Value
No. of phases	3
Rotor Type	Salient
No. of poles	2
Stator Phase Resistance	2 Ohms
Stator Inductance	L_d = 0.75H, L_q = 1.25H
Flux Linkage	0.285757 (V.s)
Inertia, Viscous damping	0.621417(g.m^2), 0.303448(mN.m. s)
DC Link Voltage	310V

4. CONCLUSION

Considerable contribution is presented by the proposed simulated model. It is expected to provide an important enhancement to the performance of electric vehicle (EV) drives through improving the RPD of IPMSM to a high resolution of 1 degree, with total error rate below 5%. This high resolution presents a significant improvement comparing with the relative works by the literature. Such resolution could essentially decrease the startup torque ripple and, consequently, lead to soft machine-running and much fewer vibrations in the power steering systems implemented in electric vehicles. Therefore, one could reliably adopt this RP detection technique to safely run the PM machines, which based on the PMSM. Although the work was simulated for two magnetic poles of IPMSM, it can be modified to be applied for any other pole-pair number. Practically, although the model might suffer from uncertainty in current measurements, adopting the average current has significantly reduced the drawbacks of this point. However, a certain technique of magnet polarity test is to be followed to enhance the resultant measurements of the proposed method by this work. Accordingly,

It can be concluded that the impulse responses due, to pulse injections, can be exploited to produce a low cost and high resolution RP detector. The work may inspire the researcher to more researching efforts in this field.

REFERENCES

[1] C. Gong, S. Member, Y. Hu, S. Member, and H. Wen, "Reliable Winding-based DC-Bus Capacitor Discharge Technique Over Full-Speed Range for IPMSM Drive in Electric Vehicles Without Position Sensor," *IEEE Trans. Ind. Electron.*, vol. 67, no. 10, pp. 8131-8142, 2020.

[2] A. S. Al-Ogaili, I. Aris, M. L. Othman, N. Azis, D. Isa, and Y. Hoon, "Design and experimental results of universal electric vehicle charger using DSP," *TELKOMNIKA Telecommunication Computing Electronics Control*, vol. 16, no. 4, pp. 1435-1444, 2018.

[3] J. Pando-Acedo, E. Romero-Cadaval, M. I. Milanes-Montero, and F. Barrero-Gonzalez, "Improvements on a sensorless scheme for a surface-mounted permanent magnet synchronous motor using very low voltage injection," *Energies*, vol. 13, no. 11, 2020.

[4] M. H. Qais, H. M. Hasanien, and S. Alghuwainem, "Low voltage ride-through capability enhancement of grid-connected permanent magnet synchronous generator driven directly by variable speed wind turbine : a review," *J. Eng.*, vol. 2017, no. 13, pp. 1750-1754, 2017.

[5] T. Mahmoud, Z. Y. Dong, and J. Ma, "Integrated optimal active and reactive power control scheme for grid connected permanent magnet synchronous generator wind turbines," *IET Electr. Power Appl.*, vol. 12, no. 4, pp. 474-485, 2018.

[6] K. Matsuoka and S. Member, "Development Trend of the Permanent Magnet Synchronous Motor for Railway Traction," *IEEJ Trans. Electr. Electron. Eng.*, vol. 2007, no. 2, pp. 154-161, 2007.

[7] S. Ali, A. Shahriari, M. Raoofat, M. Dehghani, and M. Mohammadi, "Dynamic state estimation of a permanent magnet synchronous generator-based wind turbine," *IET Renew. Power Gener.*, vol. 10, no. 9, pp. 1278-1286, 2016.

[8] S. Fang, B. Zhou, and Y. Liu, "Design and realization of dual redundancy PMSM electrical drive systems," *2009 4th IEEE Conf. Ind. Electron. Appl. ICIEA 2009*, 2009, pp. 1985-1989.

[9] B. A. Fadheel, "Design of an RLC Compensator for a Synchronous Motor: Torque Ripple Improvement," *Al-Qadisiyah J. Eng. Sci.*, vol. 12, no. 1, pp. 17–24, 2019.

[10] K. T. Chau, S. Member, C. C. Chan, C. Liu, and S. Member, "Overview of Permanent-Magnet Brushless Drives for Electric and Hybrid Electric Vehicles," *IEEE Trans. Ind. Electron.*, vol. 55, no. 6, pp. 2246-2257, 2008.

[11] A. Vagati, G. Pellegrino, and P. Guglielmi, "Comparison between SPM and IPM motor drives for EV application," in *XIX International Conference on Electrical Machines*, 2010.

[12] T. Terras and K. Hartani, "Sensorless DTC of IPMSM for embedded systems," *Int. J. Power Electron. Drive Syst.*, vol. 11, no. 1, pp. 86-96, 2020.

[13] M. Al Ibraheemi and F. Anayi, "Optimum Standstill Electronic Commutation Process for Encoderless PM Machines," *J. Eng. Appl. Sci.*, vol. 14, no. 5, pp. 8933-8939, 2019.

[14] H. Kim, S. Member, K. Huh, S. Member, R. D. Lorenz, and T. M. Jahns, "A Novel Method for Initial Rotor Position Estimation for IPM Synchronous Machine Drives," *IEEE Trans. Ind. Appl.*, vol. 40, no. 5, pp. 1369-1378, 2004.

[15] K. Ravikumar Setty, A;Wekhande, Shashank; Chatterjee, "Comparison of high frequency signal injection techniques for rotor position estimation atlow speed to standstill of PMSM," *th India Int. Conf. Power Electron.*, 2012, pp. 1-6.

[16] X. Zhou, B. Zhou, K. Wang, L. Zhang, and F. Wu, "A Novel Initial Rotor Position Estimation Strategy for Doubly Salient Electromagnetic Machine with Two Test Pulses Injetcion," *2019 22nd Int. Conf. Electr. Mach. Syst. ICEMS 2019*, 2019, pp. 8-9.

[17] K. Saleh and M. Sumner, "Sensorless control of a fault-tolerant multi-level PMSM drive," *TELKOMNIKA Telecommunication Computing Electronics Control*, vol. 16, no. 6, pp. 2930–2942, 2018.

[18] S. Mao, W. Liu, J. Peng, N. Jiao, and Y. Jiang, "Initial rotor position estimation for brushless synchronous starter/Generators," *Conf. Proc. - IEEE Appl. Power Electron. Conf. Expo. - APEC*, vol. 2019-March, 2019, pp. 1014-1017.

[19] T. Meng, W. Liu, X. Han, N. Jiao, J. Peng, and Y. Jiang, "Multi-Stage-Structure-Based Rotor Position Estimation for a Wound-Field Synchronous Starter/Generator in the Low-Speed Region," *IEEE Trans. Power Electron.*, vol. 34, no. 12, pp. 12095-12105, 2019.

[20] S. Yang, R. D. Lorenz, and T. M. Jahns, "Surface Permanent Magnet Synchronous Machine Design for Saliency-Tracking Self- Sensing Position Estimation at Zero and Low Speeds," *IEEE Trans. Ind. Appl.*, pp. 3493-3500, 2010.

[21] K. Lee and Y. Han, "MTPA control strategy based on signal injection for V/f scalar-controlled surface permanent magnet synchronous machine drives," *IEEE Access*, vol. 8, pp. 96036-96044, 2020.

[22] N. S. Pillai and R. Radhakrishnan, "Analysis And Simulation Studies For Position Sensorless BLDC Motor Drive With Initial Rotor Position Estimation," *2015 Int. Conf. Nascent Technol. Eng. F.*, 2015.

[23] X. Wu and Z. Zhu, "A Novel Rotor Initial Position Detection Method Utilizing DC-link Voltage Sensor," in *22019 IEEE International Electric Machines & Drives Conference (IEMDC), San Diego, CA, USA, 2019*, 2019, pp. 1093-1098.

[24] Q. Ni *et al.*, "A New Position and Speed Estimation Scheme for Position Control of PMSM Drives Using Low-Resolution Position Sensors," *IEEE Trans. Ind. Appl.*, vol. 55, no. 4, 2019, pp. 3747-3758.

[25] F. Anayi and M. M. A. Al Ibraheemi, "Estimation of Rotor Position for Permanent Magnet Synchronous Motor at Standstill Using Sensorless Voltage Control Scheme," *IEEE/ASME Trans. Mechatronics*, vol. 25, no. 3, pp. 1612-1621, 2020.